arXiv:nucl-th/0104006v1 2 Apr 2001

Relativistic Calculations for Incoherent Photoproduction of η Mesons

I. R. Blokland and H. S. Sherif
Department of Physics, University of Alberta
Edmonton, Alberta, Canada T6G 2J1

Abstract

We develop a relativistic model for incoherent η-photoproduction on nuclei. The elementary process is described using an effective Lagrangian containing photons, nucleons, the $S_{11}(1535)$ and $D_{13}(1520)$ nucleon resonances, and ρ, ω, and η mesons. The nucleon and η wavefunctions are obtained from relativistic wave equations. Final-state interactions of the outgoing particles are included via optical potentials. The effects of these interactions are found to be large and lead to reduced cross sections.The incoherent cross sections for isovector transitions are much larger than those for isoscalar ones. The dominant contributions are those from the S_{11} and D_{13} resonances. We find important interference effects between the contributions of these two resonances. We give some detailed calculations for the cross sections for incoherent η-photoproduction on ^{12}C. We find that the incoherent cross section for a subset of states in the excitation energy region below 17 MeV are significantly larger than those of the coherent process. These cross sections may thus be accessible experimentally.

PACS numbers: 25.20.Lj, 24.10.Jv, 24.70.+s, 13.60.Le

1 Introduction

Over the past decade, η meson photoproduction reactions have been the subject of a number of investigations, both theoretical and experimental. From a theoretical standpoint, η-photoproduction provides a useful method to examine the properties of certain nucleon resonances. In particular, since the η meson is a spin- and isospin-zero particle, its coupling to nucleons can lead to the formation of only isospin-$\frac{1}{2}$ nucleon resonances. Using nuclear targets, η-photoproduction can be used to investigate the modification of hadron properties in the nuclear medium. These reactions can also be used to study the final-state interactions of η mesons with nuclei, another topic of current interest. Reactions on nuclei can complement and further test information obtained from studying photoproduction reactions on free nucleons.

In recent years, there have been several theoretical treatments of coherent η-photoproduction reactions on nuclei. Fix and Arenhövel [1] used an effective Lagrangian approach (ELA) to examine the free η-photoproduction process, using only the $S_{11}(1535)$ and $D_{13}(1520)$ resonances, as well as t-channel vector meson exchange and nucleon pole terms. From these results, they obtained cross sections for coherent η-photoproduction on ^{4}He and ^{12}C in the near-threshold region. Peters *et al.* [2] used an ELA with a relativistic, non-local model to study coherent η-photoproduction on spin-zero nuclei. They also compared several optical potentials for the η final-state interactions. Piekarewicz *et al.* [3, 4] used a relativistic ELA to examine coherent η-photoproduction on ^{4}He, ^{12}C, and ^{40}Ca. Bennhold and Tanabe [5] used a coupled channel isobar model, in which the (γ,η) reaction is related to the (γ,π), (π,η), (π,π), and (η,η) reactions. They used the resulting elementary amplitude to study coherent and incoherent photoproduction of η mesons on nuclei. The term incoherent photoproduction, as introduced by these authors, refers to reactions leading to excited states of the final nucleus. We adopt this same definition in the present work.

The paper by Bennhold and Tanabe constitutes the only existing theoretical treatment of incoherent η-photoproduction. The small cross sections they obtained, relative to the dominant quasifree η-photoproduction process, indicate that these processes are out of reach for the current generation of experiments. Furthermore, nuclear structure complications have curtailed theoretical interest in incoherent reactions. To date, only inclusive measurements have been made for η-photoproduction on complex nuclei [6]. In order to understand the underlying mechanisms of the process better, these measurements will need to be complemented by quasifree, coherent, and incoherent measurements.

In this paper we extend a previous relativistic model for quasifree photoproduction of η mesons on complex nuclei [7, 8] to the case of incoherent η-photoproduction. The main ingredients of the present treatment are as follows. The effective Lagrangian of Benmerrouche *et al.* [9] is used for the interactions between fields. Contributions from the nucleon Born diagrams, t-channel vector mesons, and the S_{11} and D_{13} nucleon resonances are included. The nuclear wavefunctions are solutions of the Dirac equation with strong scalar and vector potentials in the spirit of the relativistic mean field theory of Walecka [10, 11]. Calculations are carried out in the plane wave approximation (PWA) and also in the distorted wave approximation (DWA) in which the final-state interactions of the η meson are taken into account.

In the following section, we outline the calculations for the amplitude and observables of an incoherent η-photoproduction reaction. In Sec. 3 we discuss the parameters that are used in the effective Lagrangian. The results of the calculations are presented and discussed in Sec. 4. Conclusions are given in Sec. 5.

2 Reaction Model

In an incoherent η-photoproduction reaction, a photon interacts with a nucleus to produce an η meson and raise the nucleus from its ground state to an excited state. In the impulse approximation, many-body contributions are neglected so that the production takes place on a single nucleon. In this approximation, the transition amplitude for the incoherent reaction $A(\gamma,\eta)A^*$ is closely related to that of the elementary reaction $N(\gamma,\eta)N$.

The starting point in the present approach is a relativistic interaction Lagrangian for a system of photons, mesons, nucleons, and nucleon resonances from which one obtains the transition amplitude for the $A(\gamma,\eta)A^*$ reaction. The amplitude is then used to calculate the observables for the reaction.

In the photoproduction of η mesons from complex nuclei, the reaction takes place within the nuclear medium. The dynamics of the nucleons within the nuclear matter are described by the relativistic mean field Lagrangian of Walecka [10, 11]. The η meson is described by solutions of the Klein-Gordon equation. The interactions of the fields involved in the reaction are described by the interaction Lagrangian

$$\mathcal{L}_{\rm INT} = \mathcal{L}_{\eta NN} + \mathcal{L}_{\gamma NN} + \mathcal{L}_{V\eta\gamma} + \mathcal{L}_{VNN} + \mathcal{L}_{\eta NR} + \mathcal{L}_{\gamma NR} \; . \tag{1}$$

We use the effective Lagrangian of Benmerrouche *et al.* [9], using pseudoscalar coupling for the ηNN vertex. The terms in (1) can be written explicitly as:

$$\mathcal{L}_{\eta NN} = -ig_{\eta NN}\overline{\psi}\gamma_5\psi\eta \ , \tag{2}$$

$$\mathcal{L}_{\gamma NN} = -e\overline{\psi}\gamma_\mu A^\mu\psi - \frac{e\kappa_p}{4M}\overline{\psi}\sigma_{\mu\nu}F^{\mu\nu}\psi \ , \tag{3}$$

$$\mathcal{L}_{VNN} = -g_v\overline{\psi}\gamma_\mu V^\mu\psi - \frac{g_t}{4M}\overline{\psi}\sigma_{\mu\nu}V^{\mu\nu}\psi \ , \tag{4}$$

$$\mathcal{L}_{V\eta\gamma} = \frac{e\lambda_v}{4m_\eta}\epsilon_{\mu\nu\lambda\sigma}F^{\mu\nu}V^{\lambda\sigma}\eta \ . \tag{5}$$

At the VNN vertex, we use a form factor of the type

$$F(t) = \frac{\Lambda^2 - m_V^2}{\Lambda^2 - t} \tag{6}$$

with $\Lambda^2 = 1.2\,\mathrm{GeV}^2$. For the S_{11} resonance,

$$\mathcal{L}_{\eta NR} = -ig_{\eta NS_{11}}\overline{\psi}R\eta + \mathrm{H.c.} \ , \tag{7}$$

$$\mathcal{L}_{\gamma NR} = -\frac{e\kappa_{S_{11}}}{2(M+M_{S_{11}})}\overline{R}\gamma_5\sigma_{\mu\nu}F^{\mu\nu}\psi + \mathrm{H.c.} \ . \tag{8}$$

For the D_{13} resonance,

$$\mathcal{L}_{\eta NR} = \frac{f_{\eta ND_{13}}}{m_\eta}\,\overline{R}^\mu\theta_{\mu\nu}(Z)\gamma_5\psi\partial^\nu\eta + \mathrm{H.c.} \ , \tag{9}$$

$$\mathcal{L}^{(1)}_{\gamma NR} = \frac{ie\kappa^{(1)}_{D_{13}}}{2M}\,\overline{R}^\mu\theta_{\mu\nu}(Y)\gamma_\lambda\psi F^{\nu\lambda} + \mathrm{H.c.} \ , \tag{10}$$

$$\mathcal{L}^{(2)}_{\gamma NR} = \frac{e\kappa^{(2)}_{D_{13}}}{4M^2}\,\overline{R}^\mu\theta_{\mu\nu}(X)\partial_\lambda\psi F^{\nu\lambda} + \mathrm{H.c.} \ , \tag{11}$$

where the tensors $V^{\mu\nu}$ and $\theta_{\mu\nu}(V)$ are defined by

$$V_{\mu\nu} = \partial_\mu V_\nu - \partial_\nu V_\mu \ , \tag{12}$$

$$\theta_{\mu\nu}(V) = g_{\mu\nu} + \left[-\frac{1}{2}\,(1+4V) + V\right]\gamma_\mu\gamma_\nu \ , \tag{13}$$

for $V = X, Y, Z$. We take $X, Y, Z = -1/2$ so that the D_{13} terms of $\mathcal{L}$ agree with Peters *et al.* [2]

At tree level, the S matrix for the $A(\gamma,\eta)A^*$ reaction is

$$S_{fi} = -\frac{1}{2}\int \langle f\,|T\left[\mathcal{L}_{\rm INT}(x)\mathcal{L}_{\rm INT}(y)\right]|i\rangle\, d^4x\, d^4y\ . \tag{14}$$

Following the procedure in [7], we obtain

$$\begin{aligned} S_{fi} &= \sum_{(j)} \frac{e}{(2\pi)^3}\sqrt{\frac{1}{2E_\eta\, 2E_\gamma}} \sum_{J_C J_B M_B} \sum_{J_{B'} M_{B'}} (J_C, J_B; M_C, M_B|J_i, M_i) \\ &\quad \times (J_C, J_{B'}; M_C, M_{B'}|J_f, M_f)\left[\mathcal{S}_{J_i J_C}(J_B)\right]^{1/2}\left[\mathcal{S}_{J_f J_C}(J_{B'})\right]^{1/2} \\ &\quad \times \int d^4x \Psi^\dagger_{J_{B'}M_{B'}}(x)\ \Gamma_{(j)}\ \Psi_{J_B M_B}(x)\ \Phi^*_\eta(x)\ e^{-ik_\gamma\cdot x}\ . \end{aligned} \tag{15}$$

In the above equation, E_γ and E_η are the energies of the photon and η meson. The struck nucleon has angular momentum quantum numbers J_B and M_B before the interaction and $J_{B'}$ and $M_{B'}$ after the interaction. J_C and M_C denote the angular momentum quantum numbers of the nuclear core, which is defined to comprise the remainder of the nucleus. The nucleus has angular momentum quantum numbers J_i and M_i before the interaction and J_f and M_f after the interaction. $(J_C, J_B; M_C, M_B|J_i, M_i)$ is a Clebsch-Gordan coefficient and $\mathcal{S}$ denotes a spectroscopic factor. $\Psi_{J_B M_B}(x)$ and $\Psi_{J_{B'}M_{B'}}(x)$ represent the wavefunctions of the bound nucleon, before and after the interaction, and $\Phi_\eta(x)$ is the η meson wavefunction. Finally, $\Gamma_{(j)}$ is a 4×4 matrix operator which contains the details of the interaction relevant to a particular reaction channel, labeled by (j). The explicit forms for $\Gamma_{\rm proton}$, $\Gamma_{S_{11}}$, $\Gamma_{D_{13}}$, and Γ_V are given in [7].

We carry out two types of calculations depending on whether or not the final-state interactions of the η are taken into account. In the PWA, we neglect final-state interactions so the η meson wavefunction takes the form

$$\Phi_\eta(x) = e^{-ik_\eta\cdot x}. \tag{16}$$

In the DWA, the η meson wavefunction is distorted through the use of an optical potential in the Klein-Gordon equation. In our DWA calculations, we will use two different optical potentials. The first optical potential, which we will denote DW1, was introduced by Lee *et al.* [12] using the ηN scattering amplitude found by Bennhold and Tanabe [5]. The second optical potential, which we will label DW3, was introduced by Peters *et al.* [2] using the results of Effenberger and Sibirtsev [13].

In order to write expressions for the observables of the reaction, we will find it useful to define a function $\mathcal{Z}$ as

$$\mathcal{Z}_{(j)} = \int d^3x \psi^\dagger_{J_{B'}M_{B'}}(\vec{x})\ \Gamma_{(j)}\ \psi_{J_BM_B}(\vec{x})\ \varphi^*_\eta(\vec{x})\ e^{i\vec{k}_\gamma\cdot\vec{x}}\ , \tag{17}$$

where ψ and φ are the spatial parts of the particle wavefunctions. Equation (15) can then be written as

$$\begin{aligned} S_{fi} \ &= \ \sum_{(j)} \frac{e}{(2\pi)^2}\sqrt{\frac{1}{2E_\eta\ 2E_\gamma}}\ \delta(E_{B'}+E_\eta-E_B-E_\gamma) \\ &\quad \times \sum_{J_CJ_BM_B}\ \sum_{J_{B'}M_{B'}} (J_C,J_B;M_C,M_B|J_i,M_i) \\ &\quad \times (J_C,J_{B'};M_C,M_{B'}|J_f,M_f)\ [\mathcal{S}_{J_iJ_C}(J_B)]^{1/2} \\ &\quad \times \left[\mathcal{S}_{J_fJ_C}(J_{B'})\right]^{1/2}\ \mathcal{Z}_{(j)}\ . \end{aligned} \tag{18}$$

The differential cross section is then related to $\mathcal{Z}_{(j)}$ by

$$\frac{d\sigma}{d\Omega_\eta} = \frac{\alpha}{8\pi}\ \frac{(2J_f+1)}{R}\ \frac{p_\eta}{E_\gamma}\sum_{(j)}\ \sum_{J_B,M_B}\ \sum_{J_{B'},M_{B'}}\ \sum_\xi \frac{\mathcal{S}_{J_iJ_C}(J_B)}{(2J_B+1)}\frac{\mathcal{S}_{J_fJ_C}(J_{B'})}{(2J_{B'}+1)}\left|\mathcal{Z}_{(j)}\right|^2\ . \tag{19}$$

Note that $\mathcal{Z}$ depends on $M_B, M_{B'}$, and the photon polarization ξ. The recoil factor R is given by

$$R = 1+\frac{E_\eta}{E_R}\left(1-\frac{p_\gamma}{p_\eta}\ \cos\theta_\eta\right)\ , \tag{20}$$

where p_γ and p_η are the momenta of the the photon and the η-meson, respectively. The photon asymmetry for linearly polarized incident photons is

$$\Sigma = \frac{d\sigma_\perp - d\sigma_\parallel}{d\sigma_\perp + d\sigma_\parallel}\ , \tag{21}$$

where $d\sigma_\perp$ and $d\sigma_\parallel$ are the differential cross sections for specified polarizations of the incident photon, namely, perpendicular and parallel to the plane of the reaction.

3 Parameters

The effective Lagrangian in Sec. 2 contains a number of parameters, such as coupling constants and anomalous magnetic moments, which must be inferred from the experimental results of other

reactions. In particular, experimental studies of the elementary η-photoproduction reaction $p(\gamma,\eta)p$ allow us to constrain our parameter set.

The parameters relating to the S_{11} and D_{13} resonances are the most crucial inputs for our effective Lagrangian. By considering the decays of these resonances through the γp and ηp channels, we can relate the parameters in equations (7) through (11) to more conventional resonance parameters [9]. For example, for the S_{11} resonance,

$$|e\kappa_{S_{11}}| = \sqrt{\frac{2M(M_{S_{11}}+M)}{(M_{S_{11}}-M)}}\ \left|A^p_{1/2}\right| \ , \tag{22}$$

$$|g_{\eta N S_{11}}| = \left(\frac{4\pi M_{S_{11}}}{p_\eta (E_N+M)}\ \Gamma_{S_{11}\to\eta N}\right)^{1/2} \ , \tag{23}$$

where $A^p_{1/2}$ is a helicity amplitude, and p_η and E_N are the momentum of the η and the energy of the nucleon, respectively, in the center of momentum frame for the decay $S_{11}\to\eta N$. Similar expressions can be written for $f_{\eta N D_{13}}\kappa^{(1)}_{D_{13}}$ and $f_{\eta N D_{13}}\kappa^{(2)}_{D_{13}}$. While these expressions specify the magnitudes of the resonance parameters, they do not provide us with any information about their phases.

In the present analysis we shall compare three slightly different sets of coupling parameters for the effective Lagrangians involving the resonances. Fix and Arenhövel [1] obtained a set of parameters that gave a good description of the elementary cross sections measured at Mainz [14]. We were able to reproduce their results using a certain set of phases for the extracted coupling parameters. As a further test of these parameters, we compared our predictions for the photon asymmetry of the elementary process to the results obtained by a recent experiment at the ESRF [15]. Figure 1 shows our prediction, along with the experimental results, for the photon asymmetry when $E_\gamma = 740\,\mathrm{MeV}$. The parameters are listed as set 1 in Table 1. Note that this set is given only for protons; the handling of neutron cross sections in this particular case is explained in the following section. Peters *et al.* [2] have also used the Fix and Arenhövel parameters to extract the coupling parameters for both protons and neutrons. The proton parameters are only slightly different from those mentioned above and the neutron parameters are based on the 1996 listings of the Particle Data Group (these are also the same in the 2000 listings). These coupling parameters are listed as set 2 in Table 1. The proton parameters in Set 3 in Table 1 are based on the recent analysis of Tiator *et al.* [16] of several observables for the photoproduction process on proton targets. This analysis produced new

parameters for the D_{13}. In particular these authors find a much smaller branching ratio than that used by Fix and Arenhövel. The rest of the coupling parameters are the same as for set 2. We shall compare the cross sections calculated using these three sets of parameters.

4 Results and Discussion

In order to put our final results into proper perspective we need to discuss two relevant issues. The cross sections for the incoherent process depend strongly on the isospin of the excited state. For isospin-zero targets we calculate these cross sections for both $T_f = 0$ and $T_f = 1$ nuclear excited states. We explain here how these calculations are done for the three sets of coupling parameters discussed above. Set 1 lists only the coupling parameters for protons (see Table 1). The calculations of the isospin dependent cross sections in this case make use of the experimental results from Mainz for η-photopoduction on the proton [14] and the deuteron [17]. An analysis by these authors, based on the dominance of the S_{11} resonance, established a neutron to proton cross section ratio. From this ratio the amplitude for the elementary process can be decomposed into isovector and isoscalar components. Specifically, based on the analysis by Krusche *et al.* [17], we take the ratio of the neutron to proton amplitudes to be -0.80. In our calculations we use the parameters of set 1 to obtain the contributions from the target protons to the incoherent amplitudes and use the above ratio to calculate the neutron contributions. These amplitudes can then be combined to yield the $T = 0$ or $T = 1$ amplitudes. This procedure is used only with set 1; sets 2 and 3 have separate coupling parameters for protons and neutron and the amplitudes are calculated independently.

The other issue that also has some bearing on the calculated cross sections is the choice of the initial and final momenta of the participating nucleon. We shall make a comparison between two choices. One is the "frozen nucleon" approximation in which each nucleon moves as part of the target but without allowance for the Fermi motion. The second, and possibly more appropriate, choice for the nucleon momenta allows for Fermi motion using an approximate model employed by other authors [18, 19, 20]. We use this model in the following form: The initial nucleon momentum in the lab frame is taken as: $\boldsymbol{p}_i = \frac{A-1}{2A}\left(\boldsymbol{p}_\eta - \boldsymbol{p}_\gamma\right)$. This choice is the same as the effective momentum used in refs [1, 5, 21]. The momentum of the nucleon in the final state is obtained by applying momentum conservation in the elementary production process.

Calculations were carried out as outlined in Sec. 2 for incoherent η-photoproduction cross sections on ^{12}C, ^{16}O, and ^{40}Ca. Qualitatively, our calculations show similar results for all three nuclei. Calculations on ^{16}O and ^{40}Ca do not produce any significant features beyond what we observe on ^{12}C. We therefore limit our discussion to the latter nucleus. We will present the results of the ^{12}C calculations, in which we have used the $1p$-shell spectroscopic factors of Cohen and Kurath [22]. We have selected four excited states of ^{12}C that are well described by a $1p_{3/2}^{-1} - 1p_{1/2}$ configuration: $(2^+0; 4.44)$, $(2^+1; 16.11)$, $(1^+0; 12.71)$, and $(1^+1; 15.11)$. It is found that transitions to the $T = 1$ states are much stronger than those to $T = 0$ states. For this reason we will present a number of comparisons below involving calculations for only the $(2^+1; 16.11)$ state. Additional calculations involving all of the four states will also be presented.

We now discuss the results of our calculations for the $^{12}\mathrm{C}(\gamma, \eta)^{12}\mathrm{C}^*(2^+1; 16.11)$ reaction. We begin by looking at the dependence of the cross sections on the choice of nucleon momenta and the sensitivity to the three coupling parameter choices discussed above. Using parameter set 1, we show in Figure 2 a comparison between the two choices of nucleon momenta. The calculations, carried out using the PWA, are presented for the differential cross section in the laboratory frame at $E_\gamma = 766\,\mathrm{MeV}$. The frozen nucleon approximation leads to larger cross sections in the forward direction than those for which the Fermi motion is taken into account in the approximate manner discussed above. The shapes of the two angular distributions are very similar. Of particular interest, though, is that the relative contributions of the S_{11} and D_{13} resonances are strongly influenced by the choice of nucleon momenta, even though the total cross sections are reasonably stable. Because the allowance for Fermi motion is the more realistic choice, all subsequent calculations in this paper are carried out with this choice.

In Figure 3 we compare the cross sections for the other two sets of coupling parameters (sets 2 and 3, Table 1). The separate contributions of the S_{11} and D_{13} are also shown. Note that in the present model the background terms do not contribute to isovector transitions, as the coupling parameters used for these terms [2] are the same for protons and neutrons. The cross sections (dotted curve) due to the S_{11} are the same for both sets since the two sets have identical parameters for this resonance. The contributions from the D_{13} are much smaller, with those from set 2 being almost double those from set 3. This reflects the small branching ratios extracted by the analysis of Tiator *et al.* [16]. This effect occurs despite the observation that the couplings $f_{\eta N D_{13}} \kappa^{(1)}_{D_{13}}$ and $f_{\eta N D_{13}} \kappa^{(2)}_{D_{13}}$

are larger for the set 3 parameters than for set 2. We have found that these two parameters give rise to amplitudes of opposite sign and that the cancellation is stronger for the set 3 parameters. One important feature evident in Figure 3 is the strong constructive interference between the S_{11} and D_{13} contributions in this energy region. Even though the D_{13} cross section is by itself small, the combined cross section is strongly enhanced (see below for a discussion of the energy dependence of this interference effect). The cross section curves in Figure 3 should also be compared with the thick solid curve in Figure 2 which gives the corresponding result for parameter set 1. We see that the latter cross section falls in between those for sets 2 and 3. This gives a measure of the adequacy of the assumption used together with set 1, namely that the isospin dependence of the total incoherent amplitude is the same as the S_{11} amplitude.

From this point on all calculations will use parameter set 3 and allow for Fermi motion. Based on the comparisons presented above, this choice, in addition to being more realistic, should provide conservative estimates of the incoherent cross sections.

It is now instructive to look at the energy dependence of the interference between the S_{11} and D_{13} contributions. For the same state as above we show the results in Figure 4, using parameter set 3 and again using plane waves for the outgoing eta particles. We see from the figure that the interference is destructive for energies near the threshold region. At photon energies above about 675 MeV the interference pattern is constructive and the influence of the D_{13} is somewhat enhanced. Calculations with sets 1 and 2 show similar behavior with slight changes in the energy at which transition from destructive to constructive interference takes place. For all parameter sets the total cross sections peak near $E_\gamma = 750\,\mathrm{MeV}$.

The cross sections in the above comparisons are calculated in the plane wave approximation in which the final-state interactions of the η mesons with the residual nucleus are neglected. In Figure 5 we study the effect of these final-state interactions. The calculations show the energy dependence of the total cross section for the same reaction on ^{12}C. The two types of optical potentials referred to earlier are used to calculate the distorted waves of the η mesons. The calculations show that the final-state interactions are substantial, leading to suppression of the cross sections particularly for photon energies near the peak region. For both distorting potentials we observe a slight shift of the cross section peak towards higher energies. At higher energies, the effects of the two optical potentials begin to diverge. The DW1 potential weakens at these energies whereas the DW3 potential retains

its strength and hence continues to suppress the cross section at these energies. The figure also shows the separate contributions from the S_{11} and D_{13} resonances for the DW1 calculations. We see that, as was the case for the PW calculations in Figure 4, the interference between these two contributions changes from destructive near threshold to constructive at higher energies.

In Figure 6, we compare the results of our calculations for the differential cross sections of the $^{12}\mathrm{C}(\gamma,\eta)^{12}\mathrm{C}^*(2^+0; 4.44)$ and $^{12}\mathrm{C}(\gamma,\eta)^{12}\mathrm{C}^*(2^+1; 16.11)$ reactions at $E_\gamma = 650\,\mathrm{MeV}$ to the corresponding calculations by Bennhold and Tanabe [5]. Our calculations use optical potential DW1 and the coupling parameters of set 3. Based on the treatment of the bound nucleons, we shall refer to our calculations as relativistic and Bennhold and Tanabe's as nonrelativistic. There is good qualitative agreement between the two sets of calculations. The relativistic calculations indicate a larger cross section for the isovector transition than the nonrelativistic calculations. The reverse holds for the isoscalar transition. Furthermore, the suppression of the cross sections due to final-state interactions is more significant in the relativistic calculations. We note however that the two approaches differ in many respects, for example, in the elementary input and the form of the transition matrix elements.

From an experimental standpoint, it would be exceedingly difficult to resolve a particular nuclear excited state left in the wake of an incoherent η-photoproduction reaction. It might be possible, however, to determine indirectly the excitation energy of the nucleus with sufficient precision to exclude coherent and quasifree reactions. To this effect, we have calculated the summed total incoherent η-photoproduction cross section on $^{12}\mathrm{C}$ for E_x in the range of 4 MeV to 17 MeV by including all four excited states mentioned at the beginning of this section. We have restricted the calculations to excitation energies where we could treat the single-particle states as bound states. Figure 7 shows this total cross section as a function of the energy of the incident photon. The curves are DWA calculations using the two optical potentials referred to earlier. This total cross section is on the order of 100 nb or more for 750 MeV photons, which is about an order of magnitude larger than several theoretical estimates of the coherent cross section[1, 2] and only about two orders of magnitude below the measured inclusive cross section for this target nucleus [6].

5 Conclusions

In this paper we have developed a relativistic model for the incoherent photoproduction of η mesons. The ingredients of the model are that (i) the nucleon wavefunctions are solutions of the Dirac equation with appropriate scalar and vector potentials consistent with the relativistic mean field approach, (ii) the η meson is described by solutions of the Klein-Gordon equation with appropriate optical potentials, and (iii) the interactions between the fields are introduced through a covariant effective Lagrangian. Contributions from the $S_{11}(1535)$ and $D_{13}(1520)$ nucleon resonances, t-channel vector mesons, and nucleon Born diagrams are included. The contributions by the latter two diagrams to the incoherent cross sections are very small.

Unlike coherent photoproduction on isoscalar targets, the S_{11} nucleon resonance provides the largest contribution to the incoherent cross section. One of the interesting results of the present work however, is the role of the D_{13} resonance. Although its cross section is evidently smaller than that of the S_{11}, the D_{13} has a significant effect on the cross section through its interference with the S_{11} contribution. We have established that this is independent of the set of coupling parameters used. The interference pattern is destructive in the threshold region, but becomes constructive at higher photon energies. The incoherent cross section is found to be much larger for isovector transitions than for isoscalar ones. This is consistent with the results of the non-relativistic calculations of Bennhold and Tanabe. We find however that the cross sections for the $T = 1$ states are somewhat larger in our calculations, while the opposite is true for the $T = 0$ transitions. Furthermore comparisons show that the suppression of the cross section due to final-state inteactions is somewhat stronger in the relativistic approach.

Although the cross sections for an incoherent η-photoproduction reaction to $T = 0$ excited states are quite small, those for $T = 1$ excited states are found to be relatively large. Our calculations show that the summed total incoherent cross sections to a set of states in ^{12}C, with excitation energies in the range $4 - 17\,\mathrm{MeV}$, are in excess of 100 nb. These are sufficiently large to be potentially observable. Such measurements would be valuable in clarifying the seemingly enhanced role played by the D_{13} in incoherent photoproduction.

Acknowledgements

We are grateful to M. Hedayati-Poor, J. I. Johansson, and R. L. Workman for helpful commu-

nications concerning their work. This work was supported in part by the Natural Sciences and Engineering Research Council of Canada.

References

[1] A. Fix and H. Arenhövel, Nucl. Phys. A **620** (1997) 457.

[2] W. Peters, H. Lenske, and U. Mosel, Nucl. Phys. A **642** (1998) 506.

[3] J. Piekarewicz, A. J. Sarty, and M. Benmerrouche, Phys. Rev. C **55** (1997) 2571.

[4] L. J. Abu-Raddad, J. Piekarewicz, A. J. Sarty, and M. Benmerrouche, Phys. Rev. C **57** (1998) 2053.

[5] C. Bennhold and H. Tanabe, Nucl. Phys. A **530** (1991) 625.

[6] M. Röbig-Landau *et al.*, Phys. Lett. B **373** (1996) 45.

[7] M. Hedayati-Poor and H. S. Sherif, Phys. Rev. C **56** (1997) 1557.

[8] M. Hedayati-Poor and H. S. Sherif, Phys. Rev. C **58** (1998) 326.

[9] M. Benmerrouche, N. C. Mukhopadhyay, and J. F. Zhang, Phys. Rev. D **51** (1995) 3237.

[10] J. D. Walecka, Ann. Phys. (N.Y.) **83** (1974) 491.

[11] B. D. Serot and J. D. Walecka, in *Advances in Nuclear Physics*, edited by J. W. Negele and E. Vogt (Plenum, New York, 1986), Vol. 16.

[12] F. X. Lee, L. E. Wright, C. Bennhold, and L. Tiator, Nucl. Phys. A **603** (1996) 345.

[13] M. Effenberger and A. Sibirtsev, Nucl. Phys. A **632** (1998) 99.

[14] B. Krusche *et al.*, Phys. Rev. Lett. **74** (1995) 3736.

[15] J. Ajaka *et al.*, Phys. Rev. Lett. **81** (1998) 1797.

[16] L. Tiator, D. Drechsel, G. Knöchlein, and C. Bennhold, Phys. Rev. C **60** (1999) 035210.

[17] B. Krusche *et al.*, Phys. Lett. B **358** (1995) 40.

[18] L. Tiator, A. K. Rej and D. Drechsel, Nucl . Phys. A **333** (1980) 343.

[19] R. Mach, Czech. J. Phys. **33** (1983) 549.

[20] S. S. Kamalov and T. D. Kaipov, Phys. Lett. B **162** (1985) 260.

[21] V. A. Tryasuchev, Phys. Atom. Nucl. **57** (1994) 379.

[22] S. Cohen and D. Kurath, Nucl . Phys. A **101** (1967) 1.

Tables

	Set 1	**Set 2**	**Set 3**
	p	p/n	p/n
$g_{\eta N S_{11}}$	2.0846	2.1/2.1	2.1/2.1
$\kappa_{S_{11}}$	-0.958	-0.962/+0.817	-0.962/+0.817
$f_{\eta N D_{13}} \kappa^{(1)}_{D_{13}}$	37.75	36.9/-6.56	42.47/-6.56
$f_{\eta N D_{13}} \kappa^{(2)}_{D_{13}}$	40.0	38.9/4.46	51.24/4.46

Table 1: $S_{11}(1535)$ and $D_{13}(1520)$ resonance parameters used in our calculations.

Figure Captions

Figure 1: The photon asymmetry Σ, as a function of the center of mass angle Θ_η, for the elementary η-photoproduction reaction $p(\gamma,\eta)p$ with $E_\gamma = 740\,\mathrm{MeV}$. The present calculations using parameter set 1 are represented by the solid line. The data points are from the ESRF experiment [15].

Figure 2: The incoherent differential cross section, as a function of the laboratory angle θ_η, for the $^{12}\mathrm{C}(\gamma,\eta)^{12}\mathrm{C}^*(2^+1; 16.11)$ reaction at $E_\gamma = 766\,\mathrm{MeV}$. The curves are PWA calculations using parameter set 1 according to the prescription explained in the text. The solid, dashed, and dash-dotted curves show the total, S_{11}, and D_{13} cross sections, respectively. The thin curves represent calculations in the frozen approximation for the struck nucleon kinematics and the thick curves show the results when Fermi motion is taken into account in the approximate manner discussed in the text.

Figure 3: Same reaction as Figure 2 except that the calculations are for parameter sets 2 and 3. The thin solid curve (set 2) and thick solid curve (set 3) are full PWA cross sections. The dotted curve shows the S_{11} cross sections (identical for both sets). The dot-dashed (dashed) curves show the D_{13} cross sections for set 2 (set 3).

Figure 4: Total incoherent cross section for the $^{12}\mathrm{C}(\gamma,\eta)^{12}\mathrm{C}^*(2^+1; 16.11)$ reaction as a function of the photon energy. The long- (short-) dashed curves show the separate cross sections of the S_{11} (D_{13}) diagrams. The calculations are carried out using the PWA and parameter set 3.

Figure 5: Total incoherent cross section for the $^{12}\mathrm{C}(\gamma,\eta)^{12}\mathrm{C}^*(2^+1; 16.11)$ reaction as a function of the photon energy. The solid curve shows the PWA calculations. The long-dashed (short-dashed) curves are distorted wave calculations using optical potential DW1 (DW3). The dotted (dash-dot) curves show the individual contributions of the S_{11} (D_{13}) resonances.

Figure 6: Differential cross sections for the $^{12}\mathrm{C}(\gamma,\eta)^{12}\mathrm{C}^*(2^+0;4.44)$ and $^{12}\mathrm{C}(\gamma,\eta)^{12}\mathrm{C}^*(2^+1;16.11)$ reactions, denoted by $T=0$ and $T=1$, respectively, with $E_\gamma = 650\,\mathrm{MeV}$. The upper graph, labeled *Relativistic*, shows the results of the present calculations using parameter set 3. The lower graph, labeled *Nonrelativistic*, shows the corresponding calculations by Bennhold and Tanabe [5]. The dashed curves indicate PWA calculations and the solid curves denote DWA calculations using the DW1 optical potential.

Figure 7: Total cross sections for the incoherent η-photoproduction reaction $^{12}\mathrm{C}(\gamma,\eta)^{12}\mathrm{C}^*$. Contributions from the $^{12}\mathrm{C}(\gamma,\eta)^{12}\mathrm{C}^*(2^+0;4.44)$, $^{12}\mathrm{C}(\gamma,\eta)^{12}\mathrm{C}^*(2^+1;16.11)$, $^{12}\mathrm{C}(\gamma,\eta)^{12}\mathrm{C}^*(1^+0;12.71)$, and $^{12}\mathrm{C}(\gamma,\eta)^{12}\mathrm{C}^*(1^+1;15.11)$ reactions are included. The curves are distorted wave calculations using DW1 (solid curve) and DW3 (dashed curve) potentials.

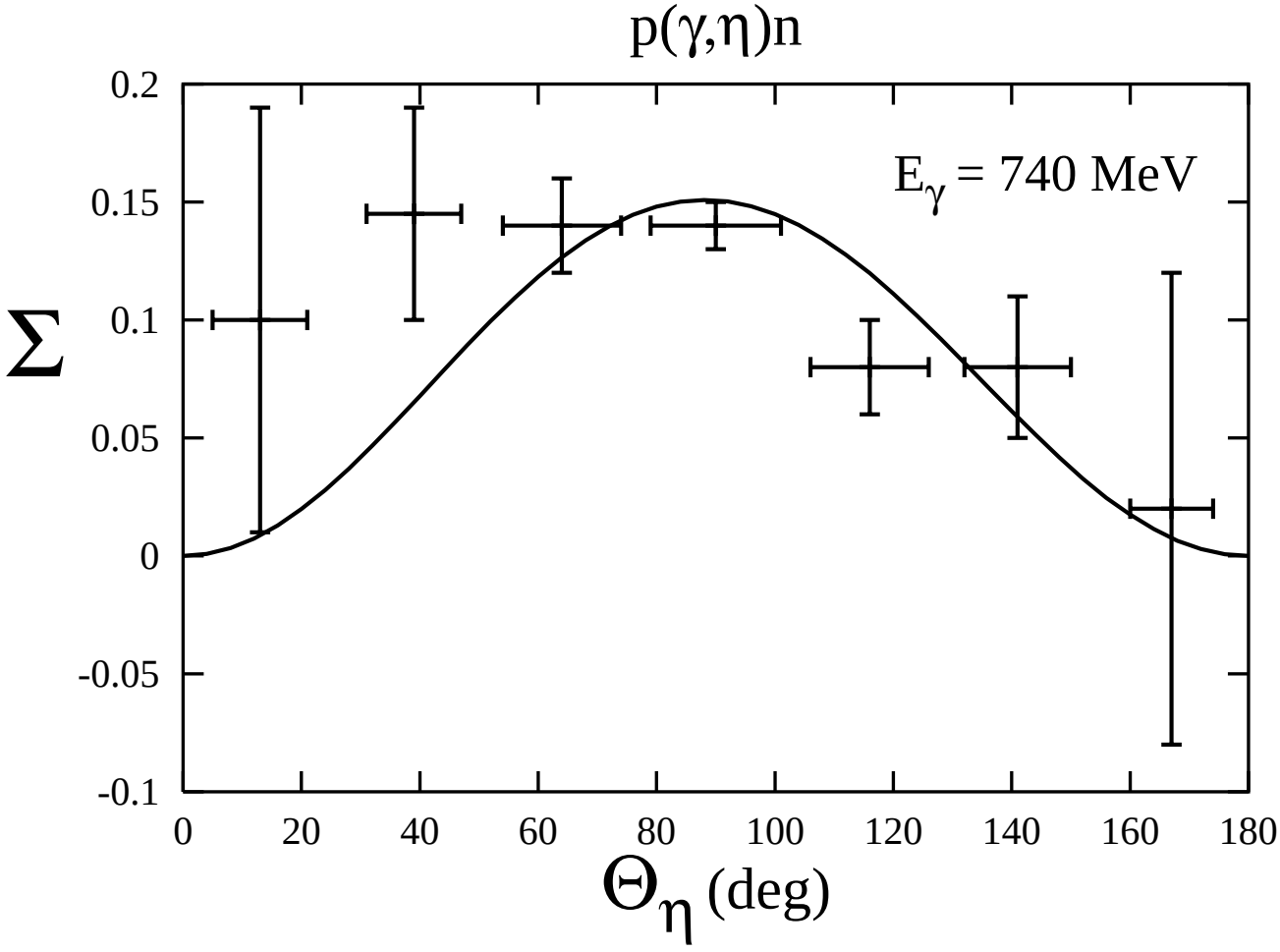
p(γ,η)n
E$_\gamma$ = 740 MeV
Σ
0.2
0.15
0.1
0.05
0
-0.05
-0.1
0
20
40
60
80
100
120
140
160
180
Θ$_\eta$ (deg)

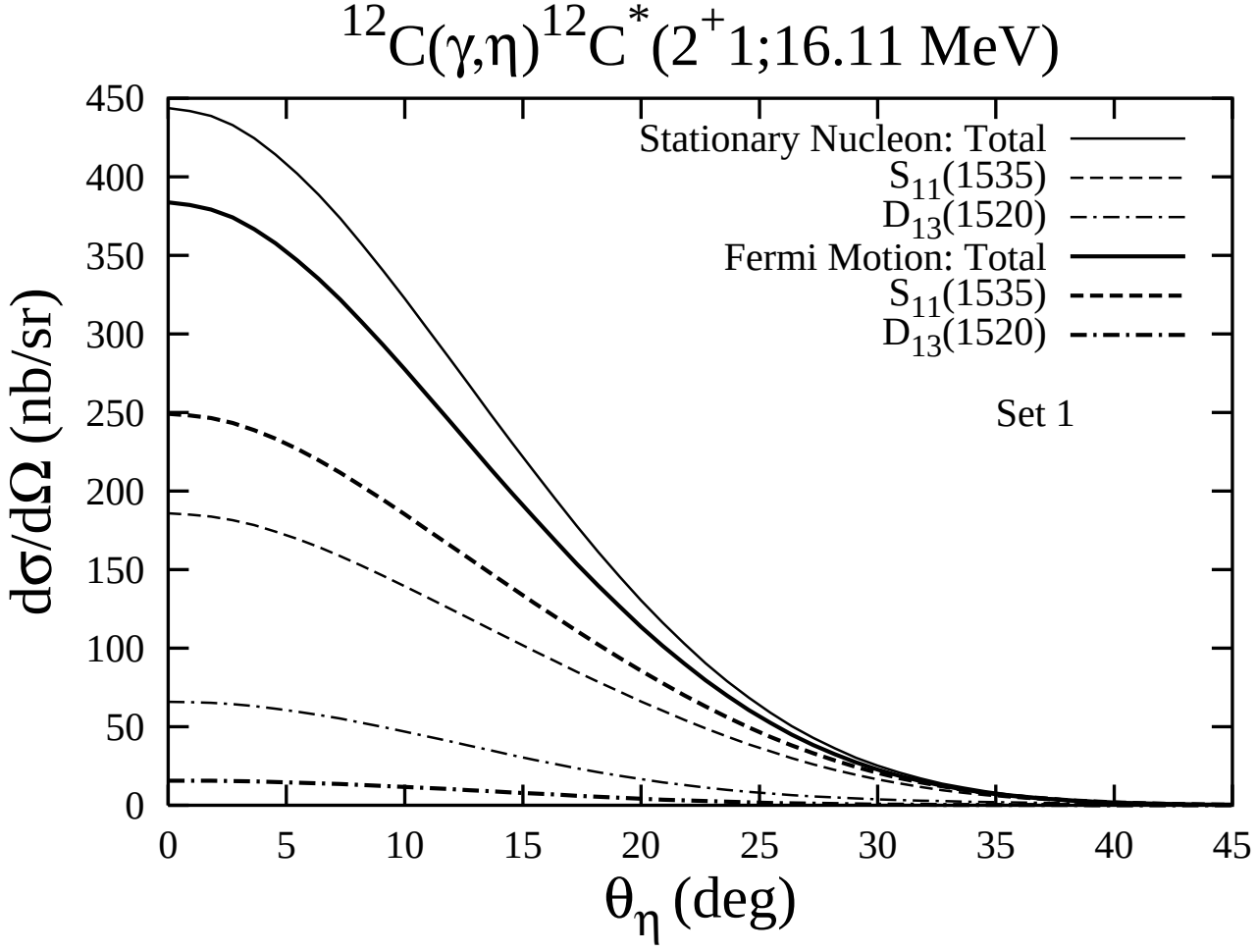
$^{12}C(\gamma,\eta)^{12}C^*(2^+1;16.11\ MeV)$
Stationary Nucleon: Total
$S_{11}(1535)$
$D_{13}(1520)$
Fermi Motion: Total
$S_{11}(1535)$
$D_{13}(1520)$
Set 1
$d\sigma/d\Omega$ (nb/sr)
θ_η (deg)
0
50
100
150
200
250
300
350
400
450
0
5
10
15
20
25
30
35
40
45

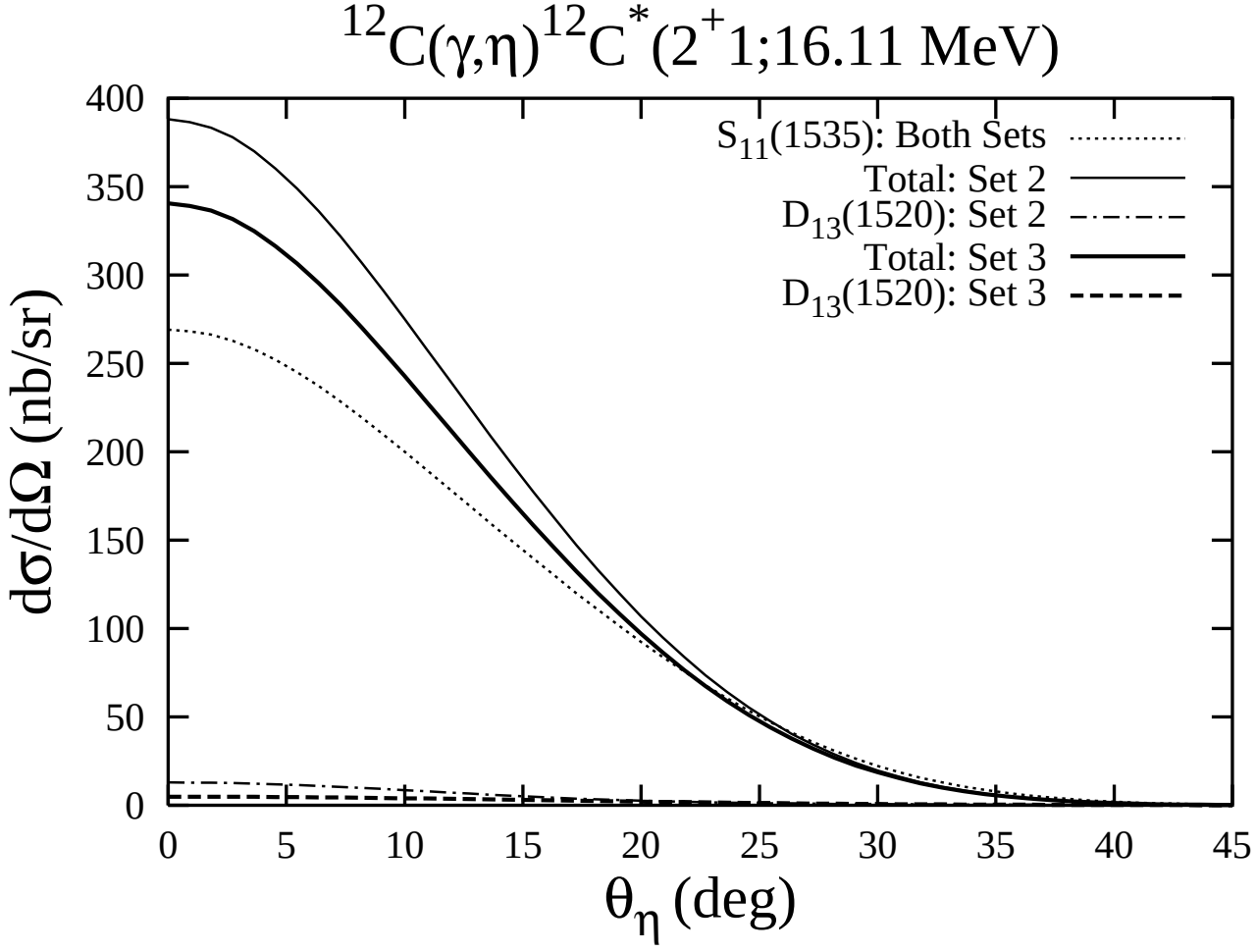
$^{12}C(\gamma,\eta)^{12}C^*(2^+1;16.11\ MeV)$
$S_{11}(1535)$: Both Sets
Total: Set 2
$D_{13}(1520)$: Set 2
Total: Set 3
$D_{13}(1520)$: Set 3
$d\sigma/d\Omega$ (nb/sr)
θ_η (deg)
0
50
100
150
200
250
300
350
400
0
5
10
15
20
25
30
35
40
45

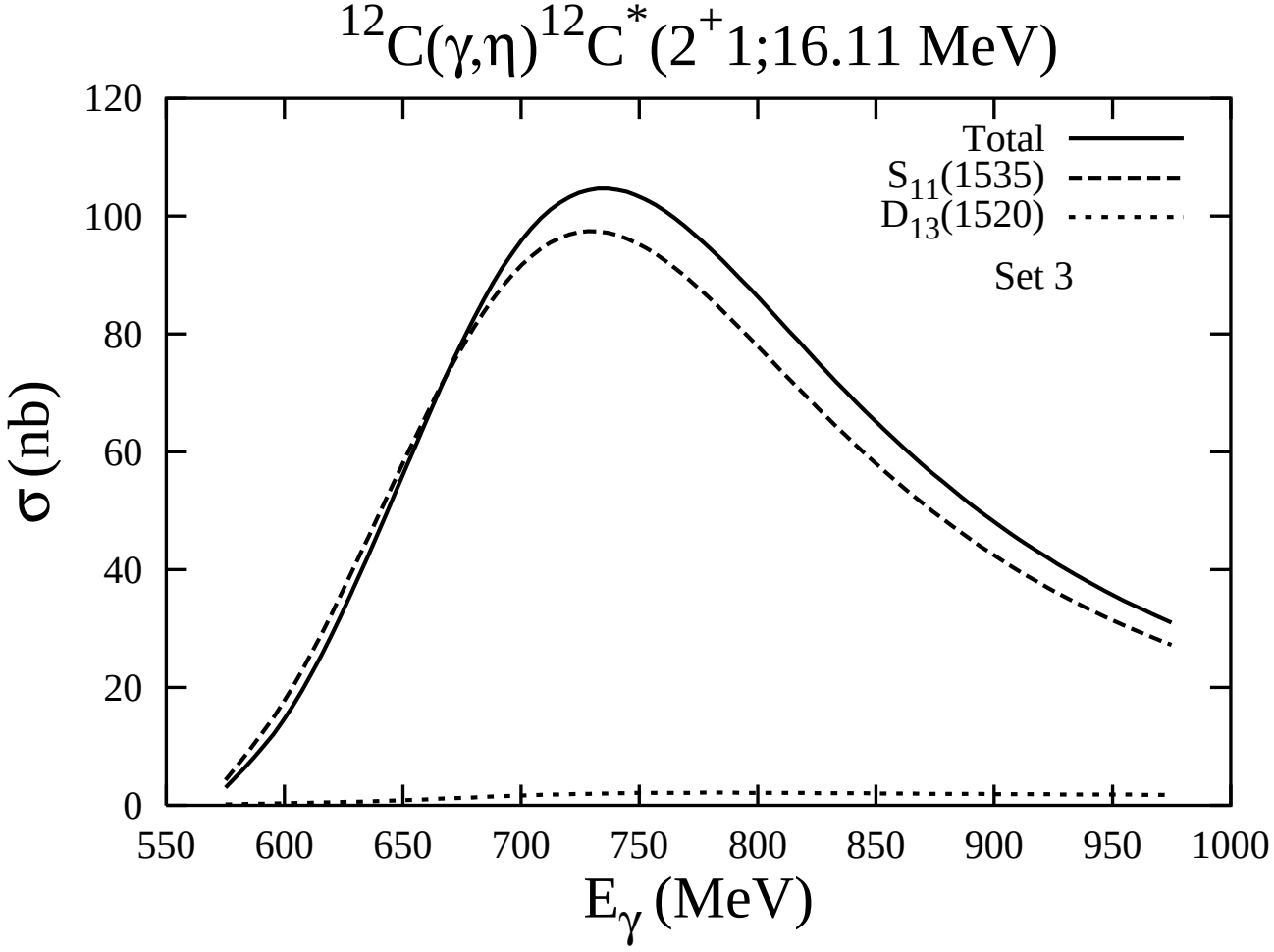
$^{12}C(\gamma,\eta)^{12}C^*(2^+1;16.11\ MeV)$
Total
$S_{11}(1535)$
$D_{13}(1520)$
Set 3
σ (nb)
E_γ (MeV)
0
20
40
60
80
100
120
550
600
650
700
750
800
850
900
950
1000

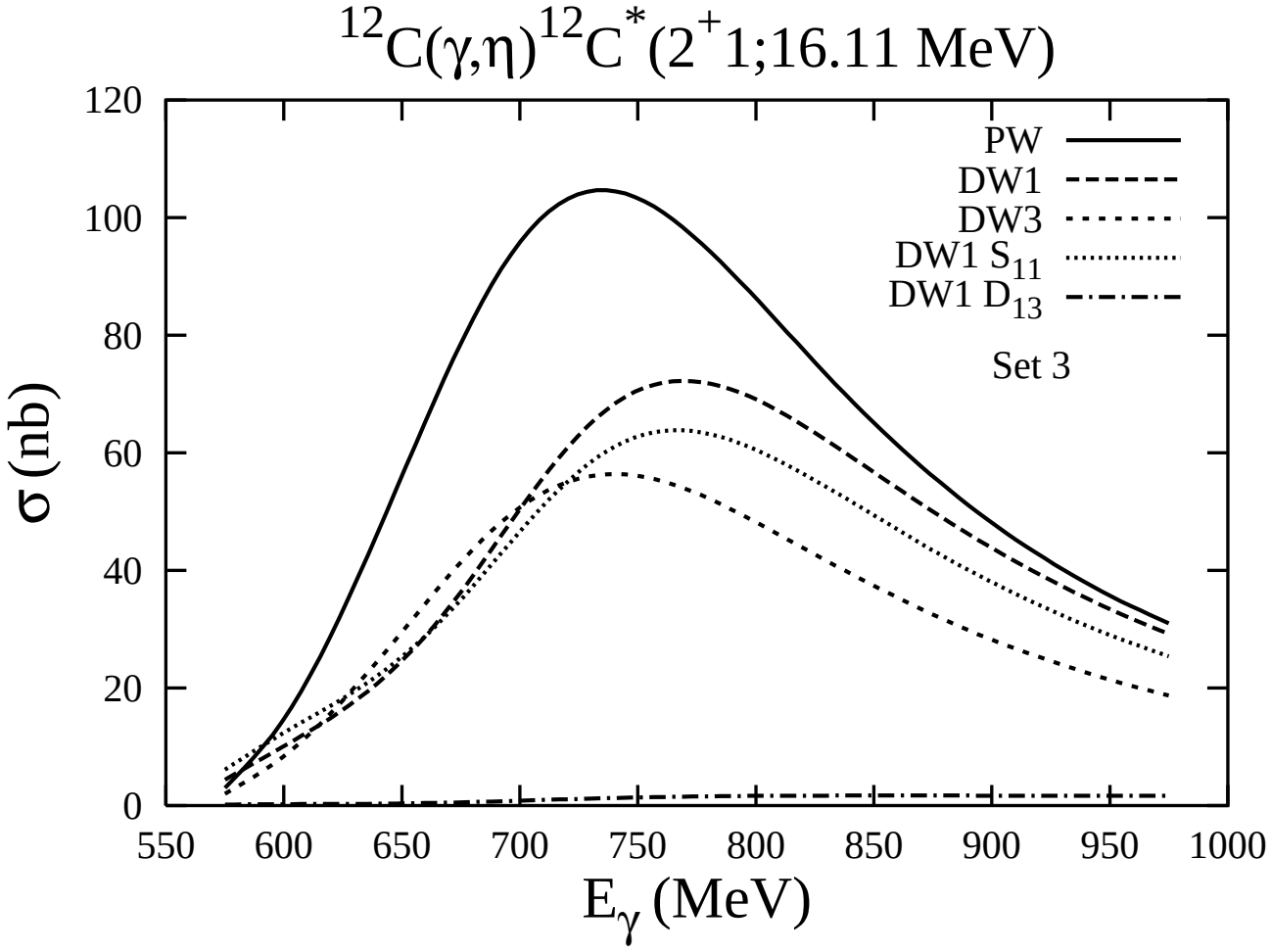
$^{12}C(\gamma,\eta)^{12}C^*(2^+1;16.11\ MeV)$
PW
DW1
DW3
DW1 S_{11}
DW1 D_{13}
Set 3
σ (nb)
E_γ (MeV)
0
20
40
60
80
100
120
550
600
650
700
750
800
850
900
950
1000

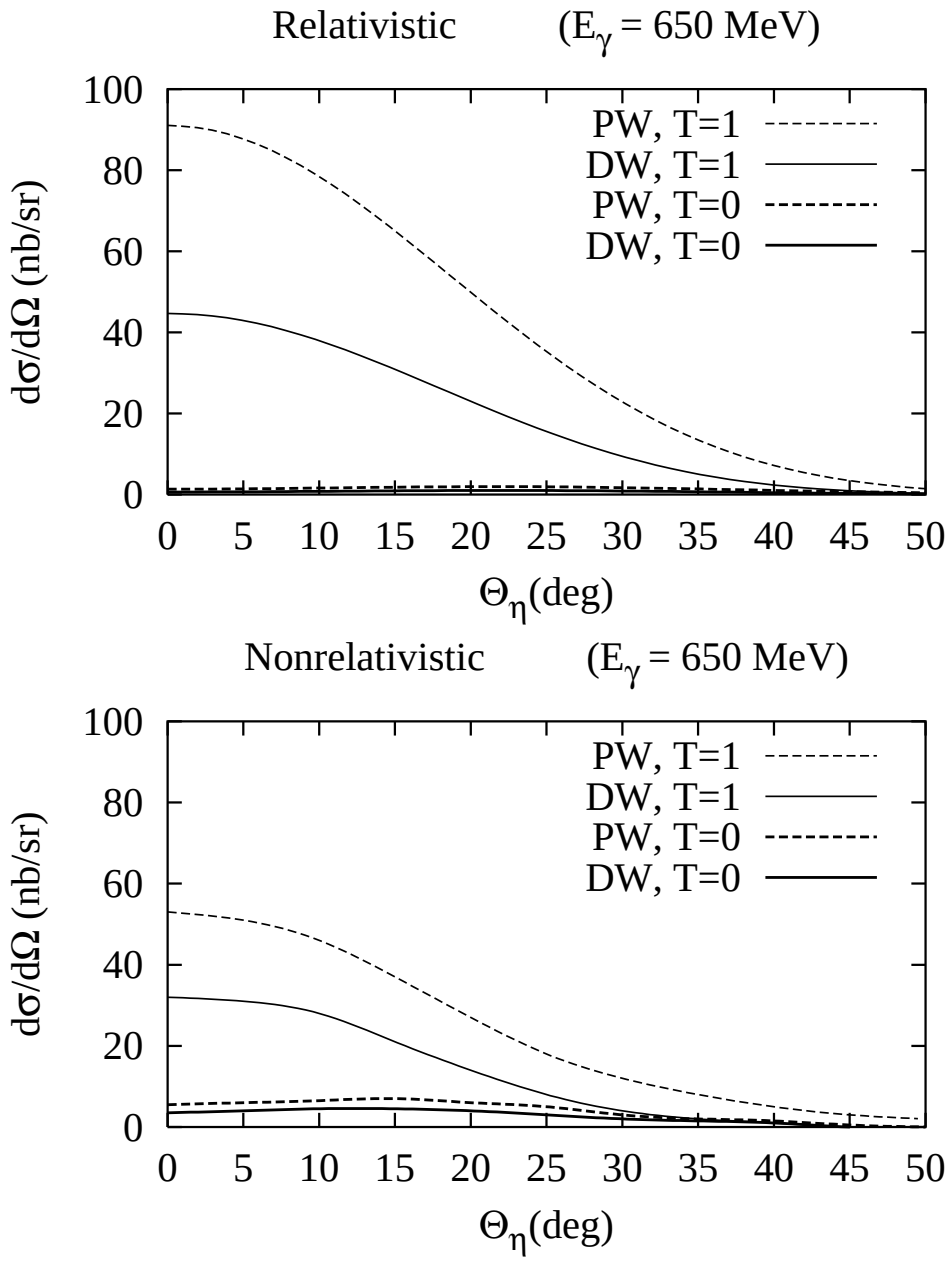
Relativistic (E$_\gamma$ = 650 MeV)
dσ/dΩ (nb/sr)
Θ$_\eta$(deg)
PW, T=1
DW, T=1
PW, T=0
DW, T=0
Nonrelativistic (E$_\gamma$ = 650 MeV)
dσ/dΩ (nb/sr)
Θ$_\eta$(deg)
PW, T=1
DW, T=1
PW, T=0
DW, T=0

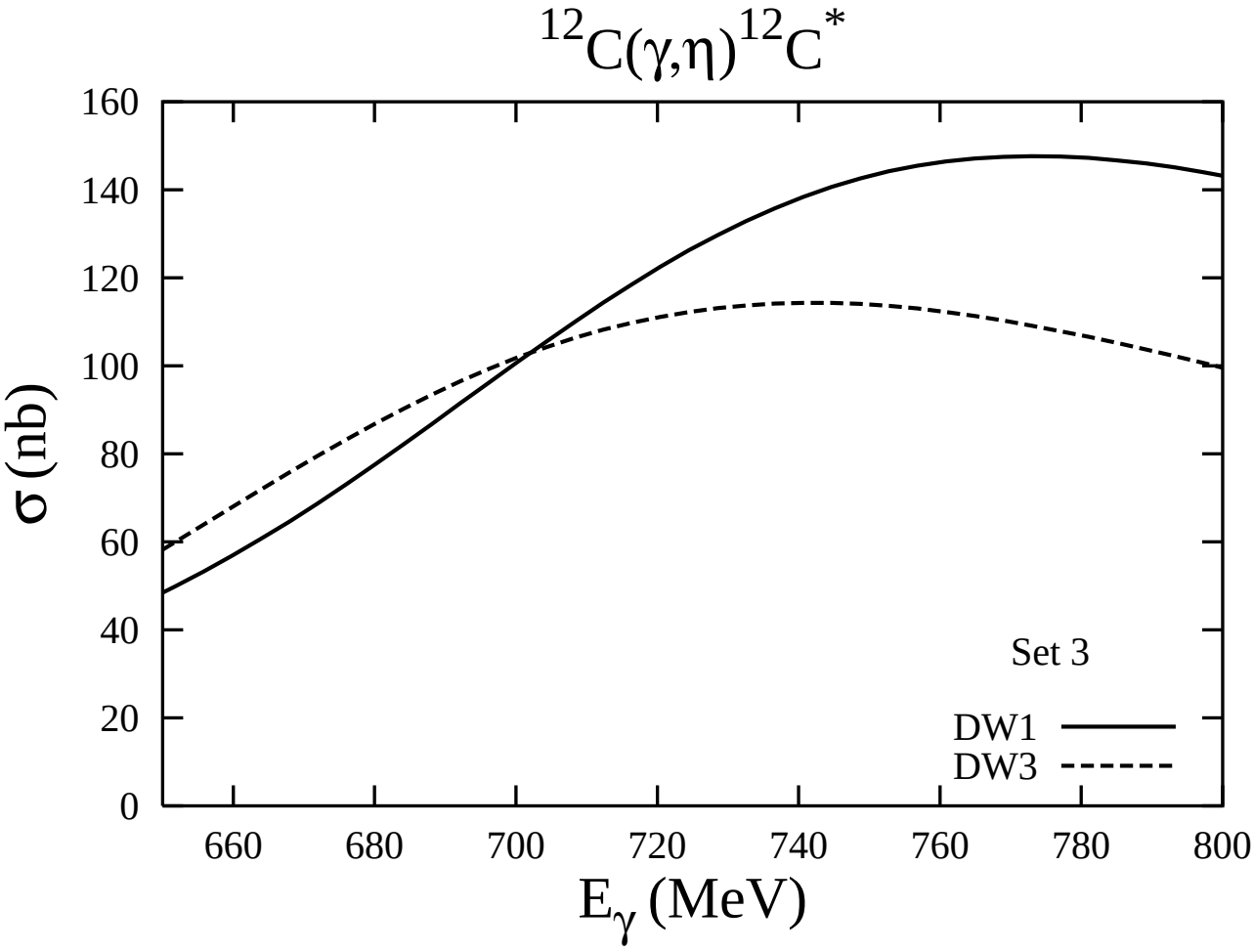
$^{12}C(\gamma,\eta)^{12}C^*$
160
140
120
100
80
60
40
20
0
σ (nb)
660
680
700
720
740
760
780
800
E_γ (MeV)
Set 3
DW1
DW3